ingegneria sismica
International Journal of Earthquake Engineering
Anno XLIII - Num. 3 - 2026

Optimization of demodulation parameters for extremely low frequency signals in optical Fiber sensors driven by optimization algorithms

Xinglong Feng[1,*]

[1] Key Laboratory of Computing Power Network and Information Security, Ministry of Education, Shandong Computer Science Center (National Supercomputer Center in Jinan), Qilu University of Technology (Shandong Academy of Sciences), 250000 Jinan, China

SUMMARY: *A demodulation parameter optimization method based on improved ant colony optimization support vector regression (IACO-SVR) algorithm is proposed to address the problems of slow demodulation speed and poor anti-interference ability of optical Fiber sensors in extremely low frequency signal demodulation. Firstly, spectral data of optical Fiber sensors under different temperature and pressure conditions were collected through experiments, and the raw data was preprocessed using Kalman filtering algorithm. Secondly, radial basis function (RBF) is used as the kernel function of SVR, and ant colony optimization algorithm (ACO) is introduced to optimize the parameters of SVR to avoid error amplification caused by the sensitivity matrix method for extremely low frequency signals. Finally, a comparative test was conducted between the IACO-SVR algorithm and the Sensitivity Matrix Method (SMM). The experimental results show that in temperature measurement, the average absolute error (MAE) of SMM is 4.99 ℃, and the average absolute percentage error (MAPE) is 14.46%; The MAE of the IACO-SVR algorithm decreased to 1.91 ℃, and the MAPE decreased to 5.61%. In terms of pressure measurement, the MAE of SMM is 2.40MPa, and the MAPE is 16.63%; The MAE and MAPE of the IACO-SVR algorithm were optimized to 0.73 MPa and 4.92%, respectively. The IACO-SVR algorithm has shown higher accuracy and stability, demonstrating the performance advantage of the proposed algorithm.*

KEYWORDS: *Optical Fiber sensor; Ultra low frequency signal demodulation; Ant colony optimization algorithm; Support Vector Regression Algorithm; Simulated annealing; Parameter optimization; Sensitivity matrix method*

1 Introduction

Optical Fiber sensors have the advantages of simple structure, high measurement accuracy, and high resonant frequency, and have potential advantages in transient pressure measurement under impact [1]. In order to measure transient sensing signals, optical Fiber sensors need to have a high dynamic frequency response. For optical Fiber sensors, their response frequency often reaches the level of extremely low frequency signals. How to quickly demodulate the cavity length and frequency response of optical Fiber sensors has become a key bottleneck limiting their application.

The traditional method of collecting spectra using a spectrometer and then using algorithms such as peak method, discrete cavity long domain transform method, Fourier transform method, and minimum mean square error method for demodulation cannot meet the requirements of fast

*19546136036@163.com
https://doi.org/10.65102/is20261128 Published: 10 June, 2026

demodulation of extremely low frequency signals due to the low line scanning speed of the charge coupled device (CCD) of the spectrometer [2]. Based on single wavelength, dual wavelength, or triple wavelength intensity methods, using single or few point high-speed detectors to collect light intensity information at the required speed is the main method for fast demodulation of optical Fiber sensors. However, for the dual wavelength and three wavelength methods, the wavelength selection must correspond one-to-one with the initial cavity length of the optical Fiber sensor, which requires high requirements for the design and manufacturing of the optical Fiber sensor. The single wavelength intensity method utilizes the linear relationship between cavity length variation and light intensity to achieve demodulation. This method is the simplest and currently the preferred method for fast demodulation of optical Fiber sensors. However, this method only relies on the intensity of a single wavelength and lacks anti-interference ability; And before use, the complete spectrum needs to be collected by a spectrometer to find the linear working area and determine the starting wavelength of the work; Switch back to using a single frequency laser as the light source for measurement. This method is complicated to operate and inconvenient for on-site testing and application. A swept frequency interference system based on a swept frequency light source and a single point detector can achieve high-speed acquisition of optical Fiber sensor signals; However, due to the limited scanning speed of the scanning light source, when the cavity length of the optical Fiber sensor varies greatly within one scanning cycle, significant demodulation errors are introduced due to the Doppler effect. The use of time-frequency analysis and fast demodulation methods based on microwave dual sideband modulation can improve the fast demodulation accuracy of optical Fiber sensors. However, due to the need for complex mathematical operations, it is difficult to obtain demodulation results immediately, and there is still a problem of inconvenient on-site application [3].

Based on the analysis of the current situation both domestically and internationally, it can be concluded that traditional demodulation methods suffer from slow demodulation speed; The intensity method has a fast demodulation speed, but it has poor anti-interference ability and inconvenient on-site application; The existing frequency scanning interferometry methods have fast acquisition speed, but there is a problem of insufficient time consumption for subsequent demodulation algorithms to meet the requirements of on-site applications. This article proposes a demodulation parameter optimization method based on improved ant colony optimization support vector regression (IACO-SVR) algorithm, aiming to optimize the demodulation parameters of optical Fiber sensors through machine learning algorithms, improve their speed and accuracy in extremely low frequency signal demodulation, and enhance their anti-interference ability to meet the needs of field applications.

2 Related research

To ensure the strength of the material is not compromised, reasonable parameter optimization must be selected when embedding large-scale FBG fiber sensors. By optimizing the parameters of FBG optical Fiber sensors [4]. The parameter optimization configuration of FBG optical Fiber sensors can not only improve the accuracy of detection, but also effectively reduce costs. For health monitoring of large structures, the parameter settings of optical Fiber sensors are crucial for the quality of data collection. Therefore, in recent years, domestic and foreign researchers have explored different parameter configuration strategies to improve the parameter setting scheme of optical Fiber sensors. These studies aim to find the optimal parameter configuration strategy for optical Fiber sensors to ensure accurate monitoring and diagnosis while maintaining structural strength. The optimized configuration of parameters enables the optical Fiber sensing network to provide more comprehensive and reliable structural state

information, providing important support for achieving structural safety and reliability.

Venketeswaran et al. proposed a fast algorithm for optimizing the coverage range of optical Fiber sensors in large grid spaces, and compared it with heuristic algorithms for placing optical Fiber sensors one by one. The performance was superior to the compared heuristic algorithms [5]. Hassani et al. monitored the strain of beam structures using FBG optical Fiber sensors with reasonable parameter settings, and obtained strain signals using FBG optical Fiber sensors, providing a new method and technical means for strain monitoring of beam structures [6]. Alabsi et al. embedded FBG optical Fiber sensors into aerospace fiber-reinforced polymers to achieve health monitoring of their structures. By setting effective parameters for the optical Fiber sensors, potential damage inside aerospace structural materials can be monitored [7]. Zaky et al. constructed a monitoring system with a minimum number of optical Fiber sensors using optical Fiber sensors, and the experiment showed that the configuration scheme of optical Fiber sensors is crucial for structural monitoring systems [8]. Maraveas improved the artificial fish swarm algorithm and applied it to optimize the configuration of optical Fiber sensing networks, effectively enhancing the measurement accuracy of FBG optical Fiber sensors [9]. Amiri et al. proposed a new method specifically for crack propagation in fiber-reinforced polymer structures using finite element analysis, optimized parameters using embedded fiber Bragg grating fiber sensors, and conducted monitoring experiments on cantilever beam cracks [10]. El Vasil et al. proposed a damage detection technique for fiber Bragg grating fiber sensor networks, which improved the damage assessment capability of the method by optimizing the parameter settings of actuators and fiber sensors [11]. Amiri et al. proposed optimization method for parameter configuration of optical Fiber sensors, with the optimization objective being the vector product of the number of optical Fiber sensors and their eigenvalues, providing a new perspective for parameter optimization of optical Fiber sensors [12]. Hoang et al. introduced an ant colony optimization algorithm with adaptive inertia weights based on the coverage optimal parameter setting criterion. And simulation experiments were conducted to optimize the parameter settings of FBG optical Fiber sensors, which further improved the convergence accuracy and speed [13]. Shadab et al. built an experimental platform and used FBG optical Fiber sensors to monitor the structural health of flexible board structures used in aerospace, which can maximize the effectiveness of structural health monitoring and improve flight safety and reliability [14]. Rovera et al. conducted stress monitoring experiments on aluminum alloy plates using multiple FBG optical Fiber sensors with parameter settings, providing a new method for monitoring and stress localization of aluminum alloy plate materials, and demonstrating the potential application value of multiple FBG optical Fiber sensors in this field [15]. Crawford et al. improved the simulated annealing algorithm by building an experimental platform for morphological reconstruction experiments, which can ensure monitoring accuracy while minimizing the number and cost of optical Fiber sensors, providing a feasible solution for the field of structural monitoring [16]. Thi et al. addressed the drawback of the standard artificial fish swarm algorithm being prone to getting stuck in local optima, and improved the algorithm by using adaptive step sizes [17]. This improved the convergence accuracy and speed of the algorithm, making the layout of FBG optical Fiber sensor nodes more reasonable. Therefore, it is very suitable for solving the parameter optimization problem of optical Fiber sensors [18]. Anuradha et al. proposed a high-precision matching algorithm based on genetic algorithm, which effectively avoids the phenomenon of premature local optima through two self-crossover methods and dynamic mutation during the mutation process. This algorithm can address each encoded optical Fiber sensor with high accuracy, promoting the application of large-scale encoding in optimizing parameter settings of fiber Bragg grating optical Fiber sensor networks.

3 Problem description

3.1 Principle analysis of optical Fiber sensors

The structure of commonly used optical Fiber sensors (such as Fabry Perot strain sensors) is shown in Figure 1. Weld a section of HCF (Changfei Company, 75 μ m/125 μ m) between two SMFs (Changfei Company, 8.2 μ m/125 μ m), with a hollow fiber length of 100 μ m. To prevent collapse of the fusion zone, optimize the discharge parameters: clean discharge time of 150ms, discharge power standard, and main discharge time of 2200ms. When the incident light enters the sensing cavity, it reflects at the M1 (SMF-HCF) and M2 (HCF-SMF) interfaces, forming interference effects.

Due to the low reflectivity of the M1 and M2 interface, the reflection field AA and normalized reflection spectrum can be represented as [19], respectively:

$$E_r = \sqrt{R_1}E_1 + (1-\gamma)(1-R_1)\sqrt{R_1}E_i e^{j(\varphi+\pi)} \tag{1}$$

$$R(\lambda) = \left|E_r / E_i\right|^2 = R_1 + (1-\gamma)^2 (1-R_1)^2 R_2 - 2\sqrt{R_1 R_2}(1-\gamma)(1-R_1)\cos\varphi \tag{2}$$

where, E_i is the intensity of the incident light field under vertical incidence conditions; φ is the interference phase difference, $\varphi = 4\pi nL/\lambda$; γ represents the diffraction loss coefficient of the light wave propagating in the air cavity; λ is the wavelength of the incident light; L represents the length of the cavity.

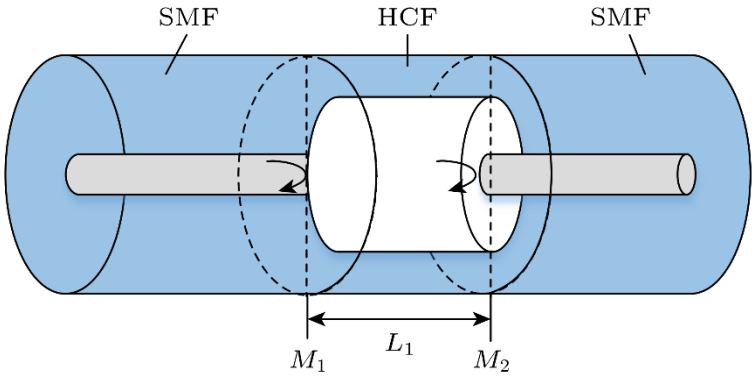

Figure 1: Optical Fiber sensor structure

When external physical quantities act on the optical Fiber sensor, the length L of the cavity and the refractive index n of the medium inside the cavity will change, resulting in a drift in the reflection spectrum. The wavelength drift of the reflectance spectrum can be expressed as [20]:

$$\Delta\lambda_m = \left(\frac{\Delta n}{n} + \frac{\Delta L}{L}\right)\lambda_m \tag{3}$$

Using a dovetail displacement platform to construct strain experiments, the optical Fiber sensor obtains uniformly distributed axial strain forces. Among them, the strain of the optical Fiber sensor is:

$$\varepsilon = \frac{L' - L}{L} = \frac{\Delta L}{L} = \frac{\Delta S}{S} \tag{4}$$

where, S represents the distance between displacement platforms, ΔS is the axial displacement of the spiral micrometer, and L' is the effective length of the cavity.

According to equations (3) and (4), it can be seen that when strain is applied to the optical Fiber sensor, the cavity length L changes. Therefore, within the strain range, the strain sensitivity of the optical Fiber sensor can be obtained by detecting the drift of a certain valley in the reflection spectrum.

In optical Fiber sensors, when the external temperature changes, the length and effective refractive index of the hollow fiber will change, resulting in a change in phase difference. According to equation (3), length and effective refractive index will cause a change in the wavelength shift of the reflection spectrum. The variation of the length and effective refractive index of the optical fiber with changes in external environmental temperature can be expressed as:

$$\Delta L = \alpha L \Delta T \tag{5}$$

$$\Delta n = \beta n \Delta T \tag{6}$$

where, α is the thermal expansion coefficient of the optical fiber, β is the thermal optical coefficient, and ΔT is the external ambient temperature.

Substituting them, we can obtain:

$$\Delta\lambda_{\mathrm{m}} = \lambda_{\mathrm{m}}(\alpha + \beta)\Delta T \tag{7}$$

The reflection spectra of optical Fiber sensors at different temperatures were simulated using Matlab. When the ambient temperature rises, the wavelength shift occurs at the trough position of the reflected spectrum, and the drift direction shifts towards longer wavelengths as the temperature increases, showing a red shift phenomenon. Therefore, suitable temperature compensation algorithms are needed to effectively eliminate the valley drift value changes caused by temperature, so that optical Fiber sensors can maintain high accuracy and stability under different temperature conditions.

3.2 Self-identification demodulation system and principle

The cavity of the optical Fiber sensor consists of two reflective surfaces with reflectivity of R_1 and R_2, respectively. The incident light beam undergoes multiple reflections inside the cavity to form multi beam interference, and the interference result formula is [21]:

$$I_{\mathrm{r}} = \frac{R_1 + R_2 - 2\sqrt{R_1 R_2}\cos\varphi}{1 + R_1 R_2 - 2\sqrt{R_1 R_2}\cos\varphi} I_0 \tag{8}$$

where, $\varphi = 4\pi nL/\lambda$. L is the length of the cavity, n is the optical index, n=1 in air, λ is the wavelength of light, and I_0 is the initial intensity of the incident light.

Non intrinsic optical Fiber sensors typically consist of optical Fiber end faces and vibration sensitive surfaces. Due to the low intrinsic reflectivity R_1 of the fiber end face and the divergence phenomenon of the cavity beam, the effective reflectivity R_2 of the vibration sensitive surface also decreases accordingly, thereby increasing the difficulty of producing high-precision fiber sensors. In addition, low precision cavity interference can be approximated as a dual beam interference model, which is convenient for demodulation. Therefore, there is more research on low precision optical Fiber sensors.

The reflectivity R_1 of the quartz air interface at the fiber end face is about 4%. For a single-mode quartz fiber operating at a wavelength of 1550nm, the total cone angle of fiber divergence is approximately 12 degrees. The effective reflectivity decreases due to divergence loss, $R_2 = \eta R_2^{'}$ (η is the divergence loss factor, $R_2^{'}$ is the effective reflectivity of the vibration sensitive surface before loss). Due to $R_1 R_2 \ll 1$, the denominator of the multi beam interference formula (8) can be approximated as 1, simplifying it to the cosine function form of dual beam interference, i.e. [22]:

$$I_r \approx I_1 + I_2 + 2\sqrt{I_1 I_2}\cos\theta = A + B\cos\theta \tag{9}$$

where, The reflected light from the fiber end face is $I_1 = I_0 R_1$, and the reflected light from the sensitive surface is $I_2 = I_0 R_2$; Considering half wave loss, the phase difference between the two beams of light is $\theta = \varphi + \pi$.

3.3 Calculation of sensitivity for demodulation of extremely low frequency signals

When the optical Fiber sensor operates at orthogonal working points, the phase sensitivity of the extremely low frequency signal is:

$$K_\varphi = B\sin\varphi_0 = B = (V_{\max} - V_{\min})/2 \tag{10}$$

The phase sensitivity B of the extremely low frequency signal can be estimated by querying the $V_{\max}$ and $V_{\min}$ values in the interference curve generated by wavelength scanning. The calculation of the sensitivity of the extremely low frequency signal is based on the assumption that the interference signal can be approximated as a cosine function model.

Another method for calculating phase sensitivity is based on the interference curve obtained by scanning the laser wavelength point by point. If it is easy to obtain the number of scanning points *N* corresponding to one interference period from the interference curve, then the phase interval between every two adjacent sampling points is $2\pi / N$. The voltage variation between adjacent points at the working point is ΔV, and the phase sensitivity of the extremely low frequency signal at the working point can be obtained as:

$$K_\varphi = \mathrm{d}I_r / \mathrm{d}\varphi = \Delta V / (2\pi / N) \tag{11}$$

Here, the unit of phase sensitivity for extremely low frequency signals is V/rad, which is the amount of voltage change caused by a unit phase change. Compared with the analytical method based on cosine model, the sensitivity estimation method for this extremely low frequency signal does not rely on the functional form of the interference signal, making it suitable for various types of optical Fiber sensors including low precision and high precision [23]. And this calculation process is independent of the absolute value of the wavelength or the specific interval value of wavelength adjustment, only requiring that the wavelength scanning interval is uniform.

When measuring vibration displacement, the cavity length $L = L_0 + \Delta L$ includes:

$$\varphi = \frac{4\pi n L}{\lambda} = \frac{4\pi n(L_0 + \Delta L)}{\lambda} = \varphi_0 + \frac{4\pi n}{\lambda}\Delta L \tag{12}$$

It can be obtained, $\Delta\varphi = 4\pi n\Delta L/\lambda$. By converting the phase sensitivity shown in equation (6) into displacement sensitivity K_S, we can obtain:

$$K_S = \frac{\mathrm{d}I_r}{\mathrm{d}L} = \frac{\mathrm{d}I_r}{\mathrm{d}\varphi} \cdot \frac{\mathrm{d}\varphi}{\mathrm{d}L} = K_\varphi \frac{4\pi n}{\lambda} = \frac{\Delta V \cdot N \cdot n}{\lambda / 2} \tag{13}$$

The center wavelength $\lambda = 1550\mathrm{nm}$ of a tunable laser and the unit of displacement sensitivity for extremely low frequency signals are $\Delta\mathrm{V/nm}$.

This method of calculating the sensitivity of extremely low frequency signals by wavelength scanning, generating and testing interference spectrum curves is a comprehensive result of the actual state of the optical path, making it simple and effective. This method has certain requirements for the laser, requiring knowledge of the number of wavelengths scanning points *N* per cycle, and the scanning range of the laser wavelength should be greater than one FSR of the optical Fiber sensor [24].

4 Optimization of extremely low frequency signal demodulation parameters based on improved ant colony optimization SVR algorithm

4.1 Algorithm Framework

The sensitivity matrix method using extremely low frequency signals may lead to the problem of amplifying system errors, resulting in unacceptable pathological matrix errors. Moreover, compared to traditional methods, machine learning algorithms have significant advantages in handling non-linear, large sample sizes, and high-precision data requirements. Secondly, the accuracy hardware of the current testing environment monitoring equipment has gradually reached a bottleneck, and every improvement in accuracy requires huge manpower and material resources. By using machine learning algorithms to optimize the data collected by the testing environment monitoring equipment, the training results can gradually approach the true value by continuously training the data on the original accuracy, thus obtaining the data closest to the true value.

This article uses machine learning methods to avoid error amplification caused by the sensitivity matrix method for extremely low frequency signals, further improving measurement accuracy. In the case of non-linear data and small sample size, support vector regression (SVR) algorithm in machine learning is used for data processing. The main principle of the SVR model is that, given a set of training data, the SVR model will represent the training data as points in space, which will be mapped to a graph. Afterwards, the SVR model will create a strip-shaped linear model function as the kernel function, and no loss will be calculated for all samples falling within the interval band; Only those outside the interval band are included in the loss function. Afterwards, the model is gradually optimized by minimizing the width of the interval band and the total loss, and the optimal solution is determined through large sample training.

By using the above method, the process is shown in Figure 2. Based on the IACO-SVR algorithm, the sensing spectrum of the optical Fiber sensor under any temperature and pressure conditions can be input into the model, thereby directly obtaining high-precision temperature and pressure values from the trained model, and solving the cross-sensitivity problem of extremely low frequency signals in multi parameter demodulation.

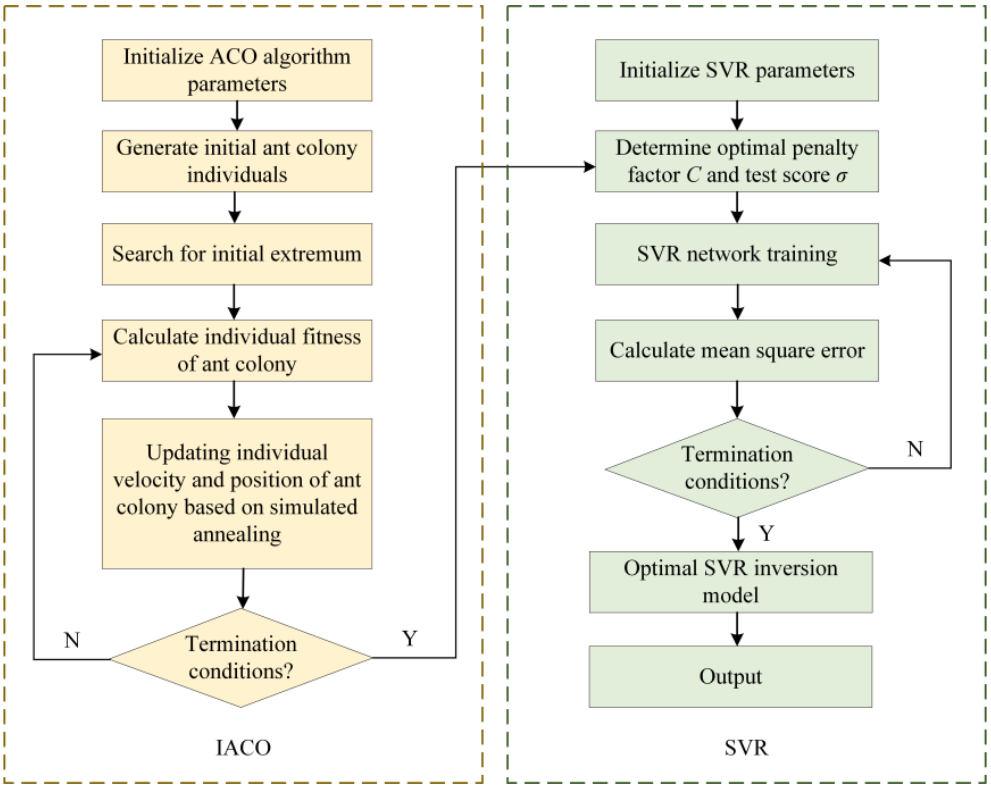

Figure 2: Algorithm Flow

4.2 SVR Model

In order to use the SVR model to predict testing environments under arbitrary temperature and pressure (T, P) conditions, a great deal of sample data is required to be obtained as input for training. After changing the temperature and pressure in the experimental testing system, this article synchronously uses a demodulator and a temperature pressure recorder (TD) to record the current spectrum and temperature pressure readings. A total of 283 spectra were collected under different temperature and pressure conditions in the experiment, of which 80% of the spectral data were randomly placed in the training set for model training, and the remaining 20% were placed in the testing set for validation to avoid data randomness.

In cases where the sample size is small and the data is non-linear, the SVR algorithm in machine learning is used for data processing. The SVR algorithm will represent the training data as points in space, which will be mapped to a graph. Afterwards, the SVR algorithm will create a strip-shaped linear model function as the kernel function, and no loss will be calculated for all samples falling within the interval band; Only those outside the interval band are included in the loss function. Afterwards, the model is gradually optimized by minimizing the width of the interval band and the total loss, and the optimal solution is determined through large sample training. Then, in the sensitivity matrix method for extremely low frequency signals, the peak information in the spectrum is used as input. In fact, the information outside the peak in the spectrum is ignored. To avoid wasting spectral information, the SVR algorithm inputs the entire spectrum and its temperature and pressure conditions into the model and calculates them. In modeling training, the kernel function used is radial basis function (RBF), which has the characteristics of stable computation time and easy adaptation to parameter optimization. RBF is shown as follows:

$$k(x, x_i) = \exp\left(\left\|x - x_i\right\|^2 / 2\sigma^2\right) \tag{14}$$

Secondly, considering that the selection of penalty factor C and parameter σ in the SVR algorithm will have a significant impact on the final fitting accuracy, ant colony optimization (IACO) algorithm is adopted to optimize the SVR parameters. The basic idea of ant colony optimization algorithm is to find the optimal solution through collaboration and information sharing among individuals in the population.

4.3 Improving Ant Colony Algorithm

(1) Standard Ant Colony Algorithm. Ant colony algorithm can search in a distributed manner, where individual ants can independently and parallelly construct solutions and communicate through pheromones to adjust routing and transmission paths. This mechanism enables ant colony algorithm to find the globally optimal routing transmission strategy in the search space, thereby significantly improving the transmission efficiency and data reliability of optical Fiber sensors in the Internet of Things. The specific process is as follows:

Step 1: Initialization operation. Randomly place *m* ants in the source node set $N=\{n_1,n_2,\cdots,n_m\}$ of the perception layer, and each virtual ant (one virtual ant representing a routing transmission strategy) selects the next node *i* to move according to a probability formula at the current node *i*.

Step 2: Probability selection. The concentration of pheromones reflects a comprehensive factor such as the frequency of past selection of this path and the reliability of transmission. The probability model of the routing transmission path is used for selection.

Step 3: Update of pheromones. This process includes two steps: volatilization and accumulation. When data is transmitted through a certain path, pheromones accumulate accordingly, indicating that the path is in good condition during transmission; During each iteration, pheromones will completely evaporate, preventing old paths from misleading subsequent node selection due to residual pheromones.

Step 4: Iterative updates. Improved probability transition rule: The original probability transition rule exposed defects in complex optical Fiber network environments. With the expansion of network scale and the increase of nodes, it is difficult to guide data towards the optimal path, and it is easy to fall into non deterministic (NP) problems with polynomial time complexity. That is, as the problem size increases, the computational complexity increases exponentially, resulting in high transmission complexity; And due to the lack of consideration for factors such as attenuation of optical Fiber sensor IoT sensing layer routing communication and uneven energy consumption of nodes, some nodes consume energy too quickly, which affects the network lifecycle, transmission stability, and real-time performance.

(2) Simulated Annealing Algorithm. The simulated annealing algorithm introduces a probability jump mechanism and a gradual cooling strategy to avoid falling into local optima during the search process, thereby achieving global optimization. The simulated annealing mechanism mainly includes the following two aspects:

1) Metropolis principle: The inner loop process is the core of simulated annealing algorithm, which allows for a certain probability of accepting poor solutions during the search process, thereby escaping from local optima, avoiding getting stuck in local minima, and improving the algorithm's ability to obtain global optima.

After iterating from the initial state, A to the local optimal solution B, even if encountering a poor solution with rising energy, it will accept the solution with a certain probability according to the Metropolis criterion, thus having the opportunity to leap out of the local optimal and improve the ability to find the global optimal solution, as shown in equation (15).

$$P = \begin{cases} 1, \Delta E < 0 \\ \mathrm{e}^{-\Delta E/T}, \Delta E \geq 0 \end{cases} \tag{15}$$

where, P represents the probability of accepting inferior solutions; ΔE represents the energy difference between the new solution and the current solution; T represents the current temperature.

When ΔE <0, the energy decreases, indicating that the new solution is better and can be directly accepted; When $\Delta E \geq 0$, the energy increases, and although the new solution is poor, it can still be accepted with a certain probability through a random mechanism to avoid falling into local optima. The specific method is to generate a random number ε. If ε<P (ΔE), the transfer is accepted.

2) Cooling criteria: i.e. external circulation process. The cooling criterion is a key mechanism that affects the simulated annealing algorithm to escape from local optima and achieve global optimization by gradually reducing the amplitude and search range of temperature control disturbances, thereby enhancing the algorithm's global search capability.

(3) Improve algorithm steps. In the measurement of large deformation displacement fields, initial value estimation plays a crucial role in the convergence speed and computational accuracy of matching algorithms. Although traditional ant colony algorithms have certain global search capabilities, they often face problems such as slow solving speed, low accuracy, and susceptibility to local optima when facing large-scale nonlinear deformations or drastic changes in image grayscale, making it difficult to meet high-precision measurement requirements. Therefore, this article will introduce coarse and fine search strategies and simulated annealing mechanisms to improve and optimize the ant colony algorithm, enhancing its search capability.

Step 1: By using the coarse and fine search method to perform grayscale cross-correlation calculation between the reference individual and the target individual, the approximate matching position of the deformation area can be quickly located over a large range. At this stage, sliding window technology is used to traverse the target image, search for the region with the highest correlation function, and use the center coordinates of this region as the initial search center for subsequent ant colony algorithms. This operation effectively reduces the dimensionality of the understanding space, minimizes invalid search paths, improves overall computational efficiency, and enhances the correlation of particle initial distributions, avoiding the problems of slow convergence or result bias in traditional ant colony algorithms without initial guidance.

Step 2: Entering the fine search stage, based on the coarse positioning results, the ant colony algorithm is used to perform fine search in the local area. In each iteration, particles continuously adjust their speed and position based on the information of their historical and global optimal positions, gradually approaching the optimal solution. In order to further enhance the global search capability of the algorithm and overcome local extremum traps. At the same time, the simulated annealing algorithm is introduced in the later stage of iteration. When the matching values corresponding to the updated particle positions are poor, the solution will still be accepted with a certain probability according to the Metropolis criterion. This probability is jointly determined by the current system temperature and the difference between the objective function, and gradually decreases with the number of iterations, forming a dynamic disturbance and convergence process. It has strong exploratory ability in the early stage and tends to stabilize in the later stage of iterations. The introduction of simulated annealing mechanism enables the algorithm to have stronger ability to leap out of local optima when facing large deformation displacement fields. Through the collaborative effect with ant colony, the diversity and adaptability of the algorithm in global search are improved, ensuring

more accurate final matching results.

Step 3: After obtaining a more accurate initial displacement value, this value is used as the initial value of the algorithm, effectively improving its convergence efficiency. Due to the sensitivity of the IC-GN algorithm to initial values, the accuracy of the initial position directly determines the speed of its iterative convergence and whether it converges to the global optimum. By utilizing the IACO to provide high-quality initial values, not only can the number of iterations required by the algorithm be reduced and the computational burden be reduced, but the accuracy of the final displacement field solution can also be improved, making the measurement results closer to the real deformation field.

5 Experimental analyses

5.1 System Construction

To contrast the precision of the IACO-SVR algorithm prediction with the sensitivity matrix method, a variable temperature and pressure experimental device was built for the optical Fiber sensor, as shown in Figure 3. Due to the circular structure of the optical Fiber sensor, light is emitted from the Optical Sensing Interrogator (OSI), passes through the uniform waist region of the optical Fiber sensor, and returns to the demodulator through the Sagnac loop at the tail. Then the demodulator will transmit the spectral information of wavelength drift that occurs in the monitoring environment to the computer, which will use the spectral information as input to run the algorithm and output the temperature and pressure under the current experimental conditions in real time.

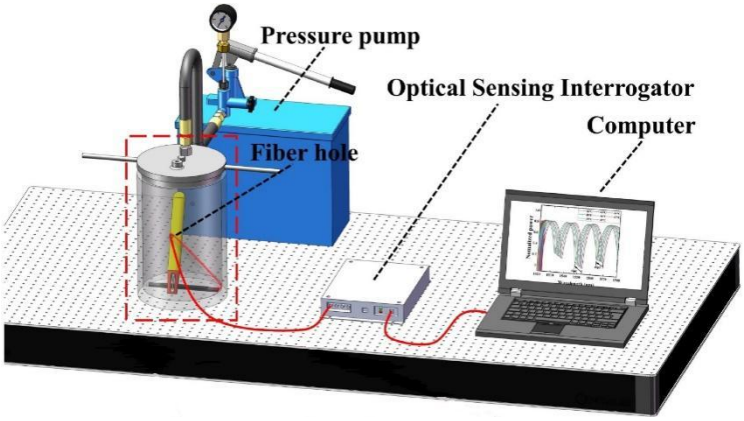

Figure 3: The structure of the variable temperature and voltage experimental system

To test the response capability of encapsulated optical Fiber sensors under variable temperature and pressure conditions, this paper simulates the testing environment by installing a tubular heating head in a pressurized sealed pressure tank. Place the optical Fiber sensor in the variable temperature and voltage experimental testing system and connect it to the demodulator through optical fiber. This optical Fiber sensor can be applied to long-term testing environment monitoring. Due to the demodulator's integrated signal guarantee processing capability of four optical Fiber sensors, it can demodulate four signals simultaneously. This optical Fiber sensor can also be spatially multiplexed over long distances. The demodulator is connected to the computer through an RJ45 interface via a network cable, and the communication protocol is UDP/IP protocol.

5.2 Data Preprocessing

During the actual measurement of optical Fiber sensors, due to external factors such as humidity and the influence of the optical Fiber sensor's own measurement, the collected data may be affected by noise interference, resulting in coarse errors in the measurement results and affecting the reliability of the measurement results [25]. This article introduces the Kalman filter algorithm to process raw spectral data. Kalman filter is a recursive optimal estimation algorithm that can dynamically estimate the system state and significantly suppress random measurement noise, given the known system state transition model and noise statistical characteristics. The core prediction and update formula of the filter is as follows:

1) Prediction steps:

$$\hat{X}_{k|k-1} = F\hat{X}_{k-1|k-1} \tag{16}$$

$$\boldsymbol{P}_{k|k-1} = F\boldsymbol{P}_{k-1|k-1}F^{\top} + Q \tag{17}$$

2) Update steps:

$$K_k = \frac{\boldsymbol{P}_{k|k-1}H^{\top}}{H\boldsymbol{P}_{k|k-1}H^{\top} + R} \tag{18}$$

$$\boldsymbol{P}_{k|k} = \left(I - K_k H\right)\boldsymbol{P}_{k|k-1} \tag{19}$$

where, $\hat{X}_{k|k-1}$ is the optimal estimate for the *k*-th measurement; $\boldsymbol{P}_{k|k}$ is the error covariance matrix; K_k is the Kalman gain; Q and R represent the covariance of process noise and observation noise, respectively. This article adopts model $F = H = 1$ and sets initial state estimation $\hat{X}_0 = 0$, initial covariance $P_0 = 1$, process noise variance $Q = 10^{-3}$, and measurement noise variance $R = 0.1$.

5.3 Algorithm Convergence Performance

To further reduce the measurement error of optical Fiber sensors and achieve temperature compensation, this paper introduces an optimized IACO-SVR to construct a temperature strain compensation model. The filtered data is input into the optimized IACO-SVR, where IACO iteratively updates the ant colony in the search space to find the optimal weight parameters. The algorithm parameters are set as follows: the maximum number of iterations is set to 1200, the specified training function is trainscg, the population size is 60, a non-linear decreasing inertia weight strategy is adopted, the learning factor is dynamically adjusted, the cognitive learning factor decreases from 2.6 to 0.5, and the social learning factor increases from 0.6 to 2.5. The weights and thresholds optimized by the IACO algorithm were used as initial parameters for SVR network training, and the training results were tested. The predicted values (red line) are highly consistent with the actual values (black line), as shown in Figure 4a, indicating that the model has high predictive ability. To objectively evaluate the performance of the model, the relative error of each sample point was calculated, and the results are shown in Figure 4b. The experimental results show that the prediction error of the optimized IACO-SVR at each sample point is smaller than that of the traditional SVR model, verifying the feasibility and superiority of the proposed method.

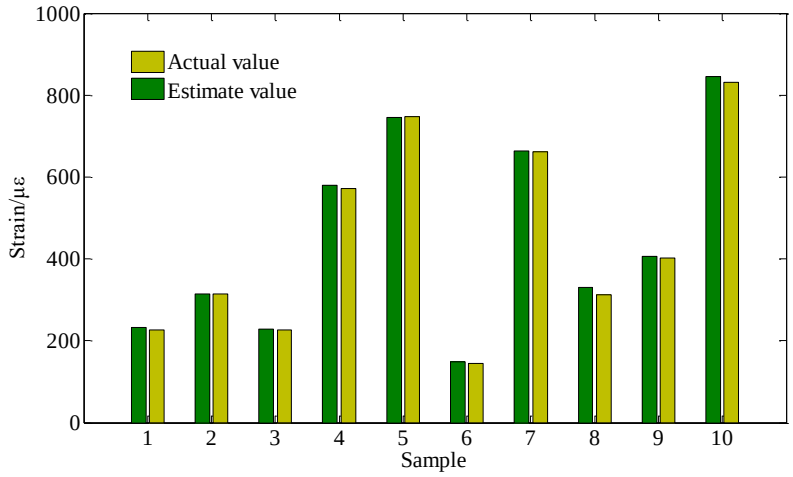

(a) Prediction output

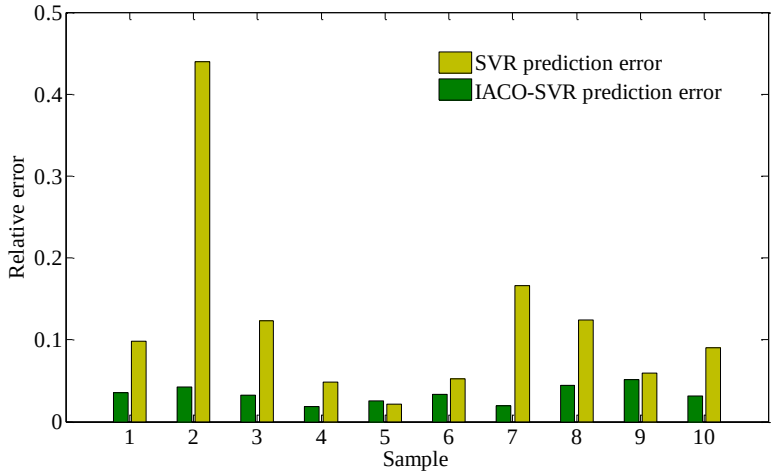

(b) Relative error

Figure 4: Training Results

5.4 Comparison of Results

The experimental test involves placing PDMS into a pressure tank, then pressurizing and heating the tank. Due to the initial increase in temperature inside the sealed tank during heating, it will cause a synchronous increase in pressure. Therefore, the data read by the temperature and depth compact recorder is used as the actual value for calibration. Every 20 minutes when the temperature and pressure inside the tank are relatively stable, the temperature and pressure inside the tank are read using a optical Fiber sensor, and the spectral data under the current temperature and pressure conditions are recorded. The error of the proposed algorithm prediction and sensitivity matrix method (SMM) under the same temperature and pressure conditions are compared, and the average absolute error (MAE) and the average absolute percentage error relative to the full range (MAPE) are calculated. The experimental results are shown in Table 1.

Table 1: Comparison of Testing Errors for Temperature and Pressure Using Different Algorithms

No.	Temperature (°C)			Pressure (MPa)		
	TD	SMM	Proposed method	TD	SMM	Proposed method
1	29.09	25.68	31.45	3.61	1.21	2.91
2	31.51	37.01	30.21	7.73	10.22	7.30
3	32.43	27.47	35.20	5.01	8.45	5.85
4	28.68	23.86	30.63	2.02	0.57	2.38
5	30.87	24.45	32.34	8.21	6.26	9.14
6	35.36	40.20	32.25	4.73	2.42	3.75
7	38.65	32.32	40.10	0.36	2.25	1.41
8	40.60	43.25	40.03	7.03	9.82	8.03
9	29.12	35.78	26.32	5.32	2.71	4.75
10	35.21	39.56	36.52	6.71	4.01	7.16
MAE	--	4.99	1.91	--	2.40	0.73
MAPE	--	14.46%	5.61%	--	16.63%	4.92%

From the data in Table 1, it can be seen that the sensitivity matrix method (SMM) generally has significant errors in temperature measurement at various test points (such as 25.68 ℃ in No.1, which deviates significantly from the actual 29.09 ℃), with an average absolute error (MAE) of 4.99 ℃ and a full-scale average absolute percentage error (MAPE) of 14.46%. By using the improved ant colony SVR algorithm, the predicted values (such as 31.45 ℃ in No.1) are closer to reality, with a significant decrease in MAE to 1.91 ℃ and MAPE to 5.61%. In terms of pressure measurement, SMM also performed poorly (such as a large deviation between No.2's 10.22MPa and the actual 7.73MPa), with a MAE of 2.40MPa and a MAPE as high as 16.63%; In contrast, MLM's MAE and MAPE were optimized to 0.73MPa and 4.92%, respectively, demonstrating higher accuracy and stability. These data fully demonstrate the superiority of MLM in temperature and pressure prediction.

6 Conclusion

This article proposes a demodulation parameter optimization method based on an IACO-SVR algorithm to address the problems of slow demodulation speed and poor anti-interference ability of optical Fiber sensors in extremely low frequency signal demodulation. Through experiments, spectral data of optical Fiber sensors under different temperature and pressure conditions were collected, and Kalman filtering algorithm was used to preprocess the raw data, effectively removing noise interference and improving data reliability. Then, radial basis function (RBF) was used as the kernel function of SVR, and ant colony optimization algorithm was introduced to optimize the parameters of SVR, avoiding the error amplification problem that may be caused by the sensitivity matrix method of extremely low frequency signals, significantly improving measurement accuracy. The experimental results show that the proposed IACO-SVR algorithm has superiority in temperature and pressure measurement, with significantly better accuracy and stability than traditional methods.

Although the IACO-SVR algorithm proposed in this article has achieved significant results in the demodulation of extremely low frequency signals in optical Fiber sensors, there are still some aspects that can be further optimized and improved. Future research will focus on the following aspects: (1) further optimizing the parameter settings of ant colony algorithm and SVR model, exploring more efficient optimization strategies to improve the convergence speed

and global search ability of the algorithm. (2) Expand the experimental dataset and add experimental samples under different environmental conditions to verify the universality and robustness of the algorithm. (3) Apply the proposed algorithm to more complex multi parameter monitoring scenarios, such as optical Fiber sensor demodulation under multi physics coupling conditions, to meet a wider range of industrial application requirements.

Author's Profile

Feng Xinglong was born in Linyi, Shandong, China. He graduated with a bachelor's degree from Shandong Institute of Business and Technology and is currently pursuing a master's degree at Qilu University of Technology, specializing in the demodulation of fiber optic sensors.

References

[1] Smailov N, Orynbet M, Nazarova A, et al. Optimization of fiber-optic sensor performance in space environments[J]. Informatyka, Automatyka, Pomiary w Gospodarce i Ochronie Środowiska, 2025, 15(2): 130-134.

[2] Subba Rao C, Geetha T S, Chellaswamy C, et al. Optimized convolutional neural network-based multigas detection using optical Fiber sensor[J]. Optical Engineering, 2021, 60(12): 127108-127108.

[3] Tiwari H, Dwivedi Y S, Singh R, et al. Exploring deep learning models aimed at favorable optimization and enhancement of optical Fiber sensor’s performance[J]. IEEE Sensors Journal, 2023, 23(17): 20330-20337.

[4] Geetha T S, Chellaswamy C, Kaliraja T. Optimized convolutional neural network-based temperature and refractive index optical Fiber sensor[J]. Journal of Optics, 2025, 54(3): 586-603.

[5] Venketeswaran A, Lalam N, Wuenschell J, et al. Recent advances in machine learning for optical Fiber sensor applications[J]. Advanced Intelligent Systems, 2022, 4(1): 2100067.

[6] Hassani S, Dackermann U. A systematic review of optimization algorithms for structural health monitoring and optimal sensor placement[J]. Sensors, 2023, 23(6): 3293.

[7] Alabsi B A, Wekalao J, Dhivya R, et al. Machine learning optimized optical surface plasmon resonance biosensor using locally weighted linear regression for rapid and accurate detection of tuberculosis biomarkers[J]. Plasmonics, 2026, 21(1): 137-164.

[8] Zaky Z A, Ahmed A M, Shalaby A S, et al. Refractive index gas sensor based on the Tamm state in a one-dimensional photonic crystal: Theoretical optimisation[J]. Scientific reports, 2020, 10(1): 9736.

[9] Maraveas C, Bartzanas T. Application of Internet of Things (IoT) for optimized greenhouse environments[J]. AgriEngineering, 2021, 3(4): 954-970.

[10] Amiri I S, Rashed A N Z, Yupapin P. Average power model of optical Raman amplifiers based on frequency spacing and amplifier section stage optimization[J]. Journal of

Optical Communications, 2023, 44(1): 19-27.

[11] El-Wasif Z, Ismail T, Hamdy O. Design and optimization of highly sensitive multi-band terahertz metamaterial biosensor for coronaviruses detection[J]. Optical and Quantum Electronics, 2023, 55(7): 604.

[12] Amiri I S, Rashed A N Z, Yupapin P. Analytical model analysis of reflection/transmission characteristics of long-period fiber bragg grating (LPFBG) by using coupled mode theory[J]. Journal of Optical Communications, 2025, 45(s1): s115-s121.

[13] Hoang V T, Boussafa Y, Sader L, et al. Optimizing supercontinuum spectro-temporal properties by leveraging machine learning towards multi-photon microscopy[J]. Frontiers in Photonics, 2022, 3: 940902.

[14] Shadab A, Raghuwanshi S K, Kumar S. Advances in micro-fabricated fiber Bragg grating for detection of physical, chemical, and biological parameters—A review[J]. IEEE Sensors Journal, 2022, 22(16): 15650-15660.

[15] Rovera A, Tancau A, Boetti N, et al. Optical Fiber sensors for harsh and high radiation environments in aerospace applications[J]. Sensors, 2023, 23(5): 2512.

[16] Crawford S E, Shugayev R A, Paudel H P, et al. Quantum sensing for energy applications: Review and perspective[J]. Advanced Quantum Technologies, 2021, 4(8): 2100049.

[17] Thi T N, Trong D H, Le Tran B T, et al. Optimization of optical properties of toluene-core photonic crystal fibers with circle lattice for supercontinuum generation[J]. Journal of Optics, 2022, 51(3): 678-688.

[18] Anuradha D, Subramani N, Khalaf O I, et al. Chaotic search-and-rescue-optimization-based multi-hop data transmission protocol for underwater wireless sensor networks[J]. Sensors, 2022, 22(8): 2867.

[19] Andrianov A V, Kalinin N A, Sorokin A A, et al. Optimizing the generation of polarization squeezed light in nonlinear optical fibers driven by femtosecond pulses[J]. Optics Express, 2022, 31(1): 765-773.

[20] Hegde G, Asokan S, Hegde G. Fiber Bragg grating sensors for aerospace applications: A review[J]. ISSS Journal of Micro and Smart Systems, 2022, 11(1): 257-275.

[21] Selvi R S, Murugesan R R, Wekalao J, et al. Advanced MXene-gold hybrid plasmonic biosensor for early detection of tuberculosis biomarkers With machine learning optimization[J]. Plasmonics, 2026, 21(1): 1441-1454.

[22] Yadav A, Kumar A, Sharan P, et al. Highly sensitive bimetallic-metal nitride SPR biosensor for urine glucose detection[J]. IEEE Transactions on NanoBioscience, 2023, 22(4): 897-903.

[23] Zeni L, Perri C, Cennamo N, et al. A portable optical-fibre-based surface plasmon resonance biosensor for the detection of therapeutic antibodies in human serum[J]. Scientific reports, 2020, 10(1): 11154.

[24] Panda A, Devi P P. Photonic crystal biosensor for refractive index based cancerous cell detection[J]. Optical fiber technology, 2020, 54: 102123.

[25] Parrish C H, Hebert D, Jackson A, et al. Optimizing spectral quality with quantum dots to enhance crop yield in controlled environments[J]. Communications Biology, 2021, 4(1): 124.